Core-shell Fe_3O_4@ZnO nanoparticles for magnetic hyperthermia and bio-imaging applications

Cite as: AIP Advances **11**, 025207 (2021); https://doi.org/10.1063/9.0000135
Submitted: 27 October 2020 • Accepted: 05 January 2021 • Published Online: 02 February 2021

Jagriti Gupta, P. A. Hassan and K. C. Barick

Core-shell Fe_3O_4@ZnO nanoparticles for magnetic hyperthermia and bio-imaging applications

Cite as: AIP Advances 11, 025207 (2021); doi: 10.1063/9.0000135
Presented: 4 November 2020 • Submitted: 27 October 2020 •
Accepted: 5 January 2021 • Published Online: 2 February 2021

Jagriti Gupta,[1,a)] P. A. Hassan,[1,2] and K. C. Barick[1,2,a)]

AFFILIATIONS

[1]Chemistry Division, Bhabha Atomic Research Centre, Trombay, Mumbai 400 085, India
[2]Homi Bhabha National Institute, Anushaktinagar, Mumbai 400 094, India

Note: This paper was presented at the 65th Annual Conference on Magnetism and Magnetic Materials.
[a)]**Authors to whom correspondence should be addressed:** jagritigupta@iitb.ac.in and kcbarick@barc.gov.in. **Tel.:** +91 22 2559 0284. **Fax:** +91 22 2550 5151

ABSTRACT

Combining two materials having different functional properties has become a current research area for biomedical applications. The progress of nanoplatforms brings new non-invasive imaging and therapeutic tools for cancer treatment. Here, multifunctional magnetic Fe_3O_4@ZnO core-shell nanoparticles (Fe_3O_4@ZnO CSNPs) have been developed by using a soft-chemical approach. Fe_3O_4@ZnO CSNPs is well characterized by X-ray diffraction (XRD), transmission electron microscopy (TEM), X-ray photoelectron spectroscopy (XPS), physical properties measurement system (PPMS), and photoluminescence spectroscopy. XRD and XPS analyses confirm the presence of both Fe_3O_4 and ZnO phases. TEM micrograph reveals that Fe_3O_4@ZnO CSNPs are spherical in shape and an average size of 10 nm. Fe_3O_4@ZnO CSNPs conserve the intrinsic superparamagnetic behavior of its constituent Fe_3O_4 with a magnetization value of ~ 31.2 emu/g. These CSNPs exhibit good heating efficacy under the applied AC magnetic field (ACMF). Further, they show a significant reduction in viability of human cervical cancer cells (HeLa) under ACMF and good fluoresecent based cellular imaging capability. Therefore, these results suggested that the multifunctional Fe_3O_4@ZnO CSNPs could be used as a promising material for image-guided magnetic hyperthermia.

I. INTRODUCTION

Metal oxide nanoparticles (NPs) have received a great deal of attention in biomedical field due to their unique physiochemical properties.[1–3] Among the others, Fe_3O_4 NPs are widely studied for magnetic hyperthermia, drug delivery, magnetic resonance imaging and magnetic separation etc.[4–6] The surface of Fe_3O_4 NPs could be easily functionalized with various organic and inorganic *moieties* which help in enhancing their properties.[3,6–8] Specifically in magnetic hyperthermia, these NPs produce heat on exposure of an alternating magnetic field (ACMF).[6,8–10] It raises the temperature of tumor to a therapeutic level (42-45 °C) and destroys cancer cells.[11–13] Further, it provides a localized treatment for the tumor without any significant damage to the surrounding healthy tissue or cells. The heating efficiency of MNPs usually reported as specific absorption rate (SAR) which depends on various factors like shape, size, phase composition and magnetic properties of particles as well as their concentration, applied magnetic field strength and frequency.[14–16] Therefore, Fe_3O_4 NPs of diverse shapes, sizes and magnetic properties are widely explored for magnetic hyperthermia therapy.[10–13]

ZnO is another important oxide having direct bandgap (3.37 eV) with large exciton binding energy (60 meV) at room temperature. ZnO NPs have been widely demonstrated for various applications including photocatalysis, biosensor, bacterial inhibitions, and drug delivery, etc.[17–21] Moreover, ZnO NPs have extensively studied as an anticancer agent, photosensitizer, and bioimaging probe due to its semiconducting characteristics, photoluminescence properties, biocompatibility, and eco-friendly nature.[22,23] Therefore, great efforts were devoted

towards the development of Fe_3O_4@ZnO core-shell nanoparticles (Fe_3O_4@ZnO CSNPs) by combining Fe_3O_4 (core) and ZnO (shell). The Fe_3O_4@ZnO CSNPs have received significant attention in the biomedical applications. Different approaches were proposed for the synthesis of Fe_3O_4@ZnO CSNPs and widely explored for drug delivery, photocatalysis and magnetic separation etc.[24–28] For instance, Zhang *et al.* investigated the therapeutic effect of transferrin receptor functionalized and DOX loaded Fe_3O_4@ZnO nanocomposites against hepatocellular carcinoma. The enhanced chemotherapeutic efficiency with excellent radiosensitizer properties of Fe_3O_4@ZnO nanocomposites was demonstrated under low dose X-ray irradiation.[26]

In this work, we have reported the synthesis of multifunctional Fe_3O_4@ZnO CSNPs by two-step soft-chemical approaches. In the first step, Fe_3O_4 core was synthesized and subsequently they were used as seed for the growth of ZnO shell over it. The structural, magnetic and photoluminescence properties of Fe_3O_4@ZnO CSNPs were investigated. They possess room temperature superparamagnetic behaviour with defect related broad visible emission. Specifically, these CSNPs exhibited significant reduction in viability of human cervical cancer cells (HeLa) under ACMF and good fluorescent based cellular imaging capability.

II. MATERIALS AND METHODS

A. Synthesis of Fe_3O_4 NPs

Fe_3O_4 NPs were prepared by hydrothermal approach using ferric (III) acetylacetonate ($Fe(acac)_3$) in triethylene glycol (TEG) solvent. In a typical process, 2 mmol $Fe(acac)_3$ in 50 ml TEG was refluxed at 250 °C under nitrogen atmosphere in a 100 mL three-neck round-bottomed flask (RBF) for 1 h in magnetic oil bath. After completion of the reaction, the oil bath was cooled to room temperature. These magnetic particles were obtained from the solvent by using a permanent magnet and thoroughly rinsed with ethanol.

B. Preparation of Fe_3O_4@ZnO CSNPs

Fe_3O_4@ZnO CSNPs were prepared by deposition of ZnO on the surface of Fe_3O_4 NPs through subsequent hydrothermal approach. The equaimolar (1:1) amount of the as-prepared Fe_3O_4 NPs and zinc acetylacetonate dihydrate ($Zn(acac)_2{\cdot}2H_2O$) was dispersed in 50 mL TEG in 100 mL RBF for 30 min and refluxed at 250 °C under nitrogen atmosphere for 30 min. After 30 min, the RBF was cooled down to room temperature. The obtained particles were washed with ethanol several times through magnetic separation and dried under vacuum oven for their structural, optical, fluorescene and magnetic characterization.

III. RESULTS AND DISCUSSION

A. Structural and microstructural analysis

The phase and structural integrity of Fe_3O_4 NPs and Fe_3O_4@ZnO CSNPs were analyzed by XRD (Fig. 1a). XRD pattern of Fe_3O_4 exhibits the cubic spinel magnetite phase with diffraction peaks at 30.20°, 35.59°, 43.22°, 54.04°, 57.25°, and 62.87°

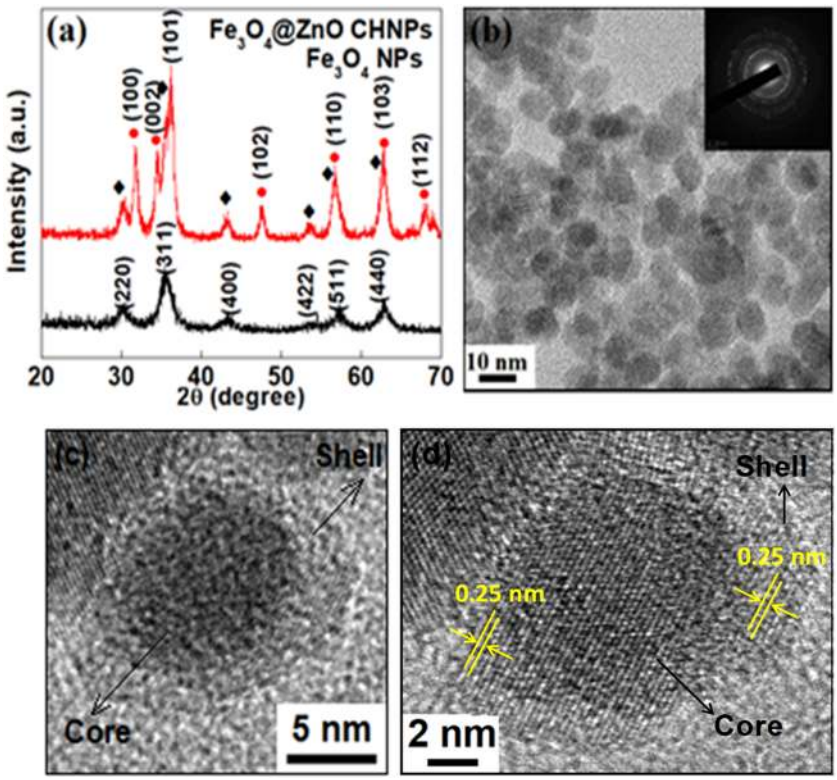

FIG. 1. (a) XRD patterns of Fe_3O_4 NPs and Fe_3O_4@ZnO CSNPs, (b-d) TEM micrographs of Fe_3O_4@ZnO CSNPs (inset of Fig. 1b shows its selected area electron diffraction partten).

corresponding to the (220), (311), (400), (422), (511), and (440) planes, respectively. XRD pattern of Fe_3O_4@ZnO CSNPs also exhibit all characteristic diffraction peaks of magnetite along with the diffraction peaks at 31.76°, 34.42°, 36.08°, 47.53°, 56.76° and 62.80° that can be indexed to (100), (002), (101), (102), (110) and (112) planes of the hexagonal wurtzite phase of ZnO. This suggests the successful formation ZnO shell without any change in phase of Fe_3O_4 nanoparticle.

From TEM micrographs (Fig. 1b and 1c), it has been found that these nanoparticles are spherical in shape and average size of 10 nm. The selected area electron diffraction partten (inset of Fig. 1b) shows the reflections corresponding to both Fe_3O_4 and ZnO phase as well as the high degree of crystallinity of sample. Here, we have used two step process for the formation of Fe_3O_4@ZnO CSNPs, where growth of ZnO layer was carried out on the surface of Fe_3O_4 through well-known seed-mediated approach.[29] The formation of core-shell nanoparticle is observed from the differences in contrast in typical TEM micrograph of Fe_3O_4@ZnO CSNPs shown in Fig 1c, where dark core can be ascribed to the Fe_3O_4 and lighter shell to the ZnO layer. From high resolution TEM (HRTEM) image (Fig. 1d), the lattice fringe of shells is measured to be ~0.25 nm corresponding to ZnO (002) plane. We could not able to see the lattice pattern of core Fe_3O_4 possibly due to the presence of thick ZnO shell. However, the dark core is clearly seen from HRTEM image. Similar, result was also observed by Lu *et al.* in Fe@Ag core-shell nanoparticle.[30]

B. X-ray photoelectron spectroscopy (XPS) analysis

XPS studies of Fe_3O_4@ZnO CSNPs was performed to confirm the presence of Fe and Zn in the sample as a supporting to XRD analysis. XPS spectrum (Fig. 2a) confirm the presence of Zn, Fe, and O in Fe_3O_4@ZnO CSNPs. The binding energy of C1s peak at 284.6 eV was used as a standard for calibration. A weak singal is observed in high resolution XPS spectrum of Fe 2p (Fig. 2b) as it is present as a core material in Fe_3O_4@ZnO CSNPs. XPS spectrum of Fe 2p shows two peaks at 709.6 and 724.5 eV corresponding to the Fe $2p_{3/2}$ and Fe $2p_{1/2}$, respectively. The appearance of sharp and symmetric peaks of Zn $2p_{3/2}$ and Zn $2p_{1/2}$ at 1020.9 and 1044.1 eV, respectively (Fig. 2b) confirm the existence of Zn in the CSNPs as Zn^{2+}.[31] XPS spectrum of O 1s (Fig 2d) could be resolved into three peaks with binding energies of 529.1, 530.3, and 531.3 eV corresponding to the lattice oxygen, surface bound oxygen, oxygen deficient region of ZnO and surface adsorbed oxygen or water molecules, respectively.[32]

C. Photoluminescence (PL) and magnetic properties

The room temperature PL and magnetic properties were studied to explore the potential applications of Fe_3O_4@ZnO CSNPs in bioimaging and hyperthermia therapy. PL spectrum (λ_{ex} = 325 nm) of Fe_3O_4@ZnO CSNPs (Fig. 3a) exhibits a UV emission peak at ~383 nm and a broad visible emission peak from 400 to 700 nm. The UV emission peak is generally ascribed to the band to band transition and the broad visible emission peak is associated with the recombination of excitons with surface oxygen defects. The most common surface defects reported in ZnO are oxygen vacancies and the intensity in the green emission depends on the concentration of the oxygen vacancies.[17,18] The appearance of strong and broad emission peak in the visible region suggests the presence of a higher concentration of defects on Fe_3O_4@ZnO CSNPs. Moreover, this

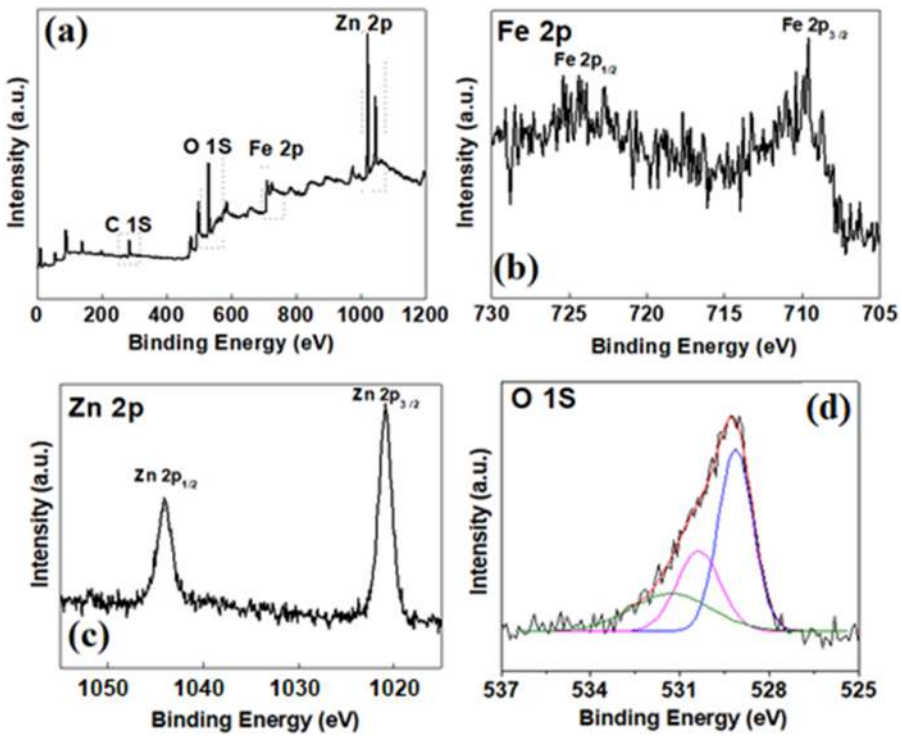

FIG. 2. (a) XPS survey scan, and high resolution XPS spectrum of (b) Fe 2p, (c) Zn 2p and (d) O 1s of Fe_3O_4-ZnO CSNPs.

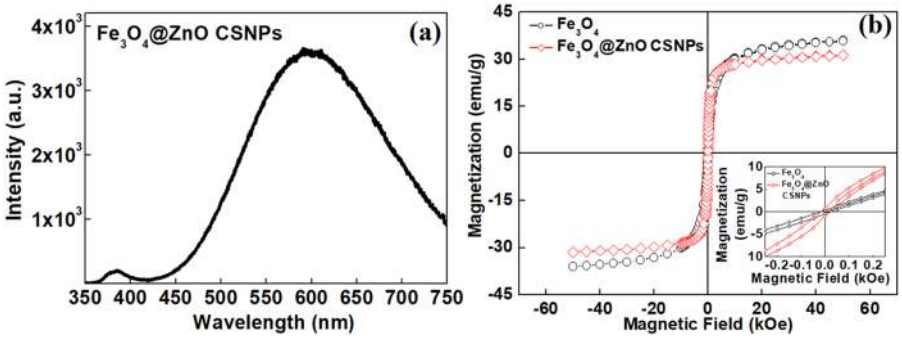

FIG. 3. Room temperature (a) photoluminescence spectra of the Fe_3O_4@ZnO CSNPs (λ_{ex} = 325 nm) and (b) field-dependent magnetization plots of Fe_3O_4 NPs and Fe_3O_4@ZnO CSNPs (inset shows its expanded plot at low field region).

strong emission in the visible region makes these CSNPs promising candidates for bioimaging.[33,34]

From field-dependent magnetization plots (Fig. 3), it has been observed that the magnetization response of both Fe_3O_4 and Fe_3O_4@ZnO CSNPs is steep and almost linear at low fields region (as the particles start to align with the applied magnetic field), whereas the particles are almost aligned with the applied magnetic field and the magnetization approaches saturation at higher fields. The coercivity and remanence of Fe_3O_4 NPs were found to be 15 Oe and 0.3 emu/g, while those of Fe_3O_4@ZnO CSNPs were 17.5 Oe and 0.8 emu/g, respecitvely. The appearance of negligible coercivity and remanence suggests that these samples possess superparamagnetic behaviour at room temperature. Further, the mximum magnetization value of Fe_3O_4@ZnO CSNPs (31.2 emu/g) was found to be slightly lower than that of Fe_3O_4 NPs (35.8 emu/g) at 5 T. From magnetization, it has been found that the ZnO shell in Fe_3O_4@ZnO CSNPs contributes to a decrease in magnetization value of Fe_3O_4 of about 12%. Therefore, the retention of good magnetic field responsivity of Fe_3O_4@ZnO CSNPs driven us to explore their heating efficacy for hyperthermia application.

D. Magnetic heating efficacy

The heating efficacy of aqueous suspensions of Fe_3O_4 and Fe_3O_4@ZnO CSNPs (1 mg/mL of Fe) were performed by the time-dependent calorimetric measurements under ACMF of 315 Oe and frequency of 250 kHz (Fig. 4a). A gradual increase in temperature as a function of time is observed for both Fe_3O_4 NPs and Fe_3O_4@ZnO CSNPs. The applied ACMF and frequency is capable to produce adequate energy for increasing the temperature of 1 mg/mL of Fe to the hyperthermia therapeutic regime. The SAR values of Fe_3O_4 NPs and Fe_3O_4@ZnO CSNPs were found to be 92.0 and 80.0 W/g, respectively (inset of Fig. 4a). The heating efficacy of these superparamagnetic nanoparticles under ACMF can be attributed to the Brownian and Néel relaxation loss processes.[35] Further, we have also calculated the system-independent ILP as SAR values are dependent on the applied field strength and frequency. The ILP values of Fe_3O_4 NPs and Fe_3O_4@ZnO CSNPs were found to be 0.58 and 0.49 nHm^2/Kg, respectively. These ILP values are in the range of those reported for commercial ferrofluids.[34] Specifically, the prepared Fe_3O_4@ZnO CSNPs can be used as efficient heating source for magnetic hyperthermia applications.

E. Cellular studies

The effect Fe_3O_4 NPs and Fe_3O_4@ZnO CSNPs on viability of HeLa cells was investigated by SRB assay (Fig. 5a). After incubation for 24 h, it was observed that Fe_4O_3 NPs do not show any significant change in the viability of HeLa cells up to a concentration of 1 mg/mL (1000 μg/mL). However, Fe_3O_4@ZnO CSNPs are not biocompatible with HeLa cells and has toxicity concerns. It exhibits toxicity at higher concentrations (125 to 1000 μg/mL), which could be associated with the presence of ZnO shell and its role in production of reactive oxygen species (ROS).[19] Having noted the good heating efficiency of Fe_3O_4@ZnO CSNPs, we have also investigated their hyperthermia effect on HeLa cells in presence and absence of ACMF (Fig. 5b). It was observed that the control cells (untreated) and cells treated with ACMF only did not show much change in the percentage cell viability. However, Fe_3O_4@ZnO CSNPs under 5 min exposure of ACMF showed about 50% reduction in cell viability for 1 mg/mLof Fe as compared to the ~25% decrease with particle only under similar condition. Further, cell viability is reduced from 50 to 25% when treatment time was increased from 5 to 15 min. It is

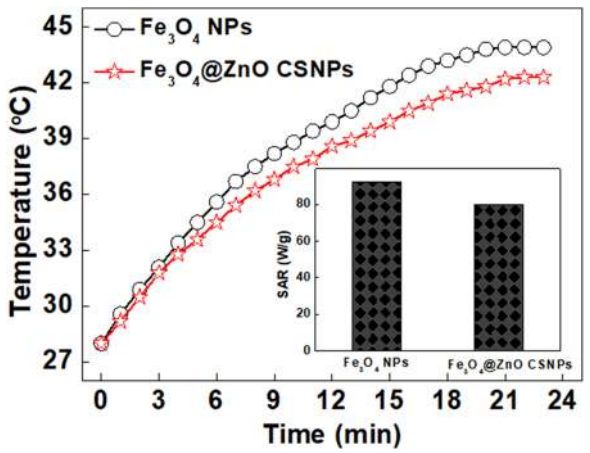

FIG. 4. Temperature vs. time plots of aqueous suspensions of Fe_3O_4 and Fe_3O_4@ZnO CSNPs (1 mg/mL of Fe) under applied ACMF of 315 Oe and frequency of 250 kHz (insect shows the SAR values of Fe_3O_4 NPs and Fe_3O_4@ZnO CSNPs).

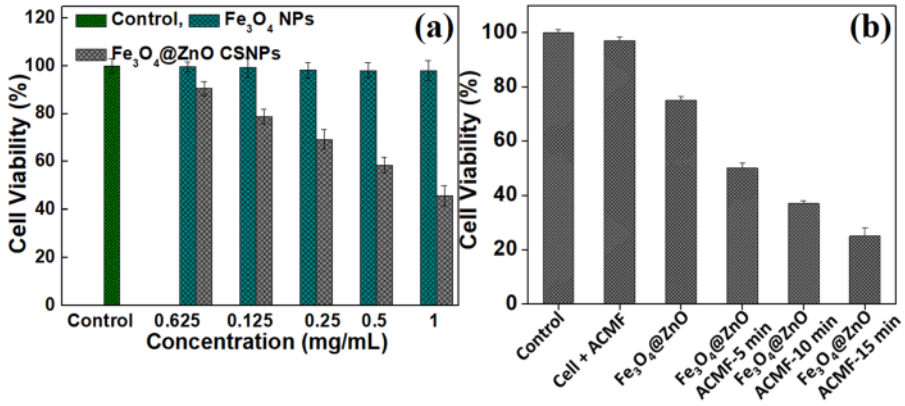

FIG. 5. (a) Viabilities of HeLa cells in presence of different concentrations of Fe_3O_4 NPs and Fe_3O_4@ZnO CSNPs after incubation at 37 °C for 24 h, and (b) viabilities of HeLa cells upon treated with Fe_3O_4@ZnO CSNPs (1 mg/mL of Fe) in presence and absence of ACMF.

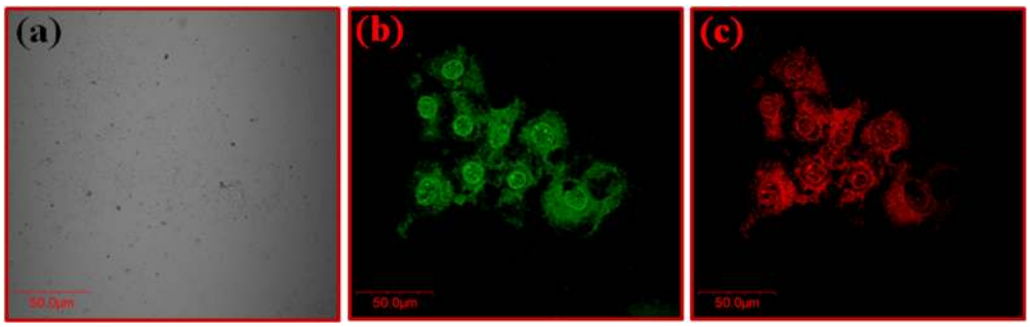

FIG. 6. Confocal microscopy (a) bright field, (b) green fluorescence and (c) red fluorescence images of HeLa cells treated with Fe_3O_4@ZnO CSNPs for 4 h under culture conditions.

noteworthy to mention that the results of Fig. 5a and 5b should not compare with each other as both the experiments were performed at different conditions.

Furthermore, the cellular imaging of Fe_3O_4@ZnO CSNPs was investigated by confocal microscope using HeLa cells (Fig. 6a-6c). As shown in Fig. 6b and 6c), a large number of Fe_3O_4@ZnO CSNPs (shown in green and red, due to braod emission from 400 to 700 nm) were distributed in the cytoplasmic region after the initial incubation for 4 h. It has been observed that the Fe_3O_4@ZnO CSNPs are well distributed and accumulated in the cell cytoplasm and nucleus. Specifically, the present study demonstrates the potential of Fe_3O_4@ZnO CSNPs for hyperthermia therapy and cellular imaging.

IV. CONCLUSION

We have successfully reported the synthesis of Fe_3O_4@ZnO CSNPs by the two step hydrothermal approach in triethylene glycol solution. XRD and TEM analysis confirm the formation of inverse spinal phase for Fe_3O_4 and hexagonal wurtzite phase for ZnO in spherical size. The PL spectrum of Fe_3O_4@ZnO CSNPs show strong photoluminescence property which is very promising for bioimaging application. Moreover, the magnetization and magnetic heating efficacy studies showed that Fe_3O_4@ZnO CSNPs exhibit a superparamagnetic behavior at room temperature and excellent heating profile, respectively. Overall, the multifunctional Fe_3O_4@ZnO CSNPs have shown significant potential for their use in magnetic hyperthermia and bio-imaging.

SUPPLEMENTARY MATERIAL

See supplementary material for the elaborate experimental procedure for cell viability, cellular imaging, magnetic hyperthermia studies and material characraterization details.

ACKNOWLEDGMENTS

Dr. Jagriti Gupta acknowledges the Department of Science and Technology (DST), Government of India for the award of Women Scientist Fellowship (Grant No. SR/WOS-A/CS-146/2018). The authors are thankful to the Centre for Research in Nanotechnology & Science (CRNTS) and Central Facility, IIT Bombay for TEM. The authors are also thankful to Prof. D. Bahadur, IIT Bombay for facilitating TEM, XPS and magnetic measurements.

DATA AVAILABILITY

The data that support the findings of this study are available within the article.

REFERENCES

[1] A. Sangtani, O. K. Nag, L. D. Field, J. C. Breger, and J. B. Delehanty, Nanomed. Nanobiotechnol. **9**, e1501 (2017).
[2] B. Liu and J. Liu, TrAC Trends Anal. Chem. **121**, 115690 (2019).
[3] S. Chandra, K. C. Barick, and D. Bahadur, Adv. Drug Del. Rev. **63**, 1267 (2011).
[4] G. Yang, S. Z. F. Phua, A. K. Bindra, and Y. Zhao, Adv. Mater. **31**, 1805730 (2019).
[5] V. F. Cardoso, A. Francesko, C. Ribeiro, M. Bañobre-López, P. Martins, and S. Lanceros-Mendez, Adv. Healthcare Mater. **7**, 1700845 (2018).
[6] J. Gupta, J. Mohapatra, P. Bhargava, and D. Bahadur, Dalton Trans **45**, 2454 (2016).
[7] D. Dutta, J. Gupta, D. Thakur, and D. Bahadur, Mater. Res. Express **4**, 125005 (2017).
[8] J. Gupta, A. Prakash, M. K. Jaiswal, A. Agarrwal, and D. Bahadur, J. Magn. Magn. Mater. **448**, 332 (2018).
[9] B. Dutta, A. Nema, N. G. Shetake, J. Gupta, K. C. Barick, M. A. Lawande, B. N. Pandey, I. K. Priyadarsini, and P. A. Hassan, Mater. Sci. Eng. C **112**, 110915 (2020).
[10] J. Mohapatra, S. Nigam, J. Gupta, A. Mitra, M. Aslam, and D. Bahadur, RSC Adv **5**, 14311 (2015).
[11] J. Gupta, P. Bhargava, and D. Bahadur, J. App. Phys. **115**, 17B516 (2014).
[12] F. Shubitidze, K. Kekalo, R. Stigliano, and I. Baker, J. App. Phys. **117**, 094302 (2015).
[13] E. Kita, T. Oda, T. Kayano, S. Sato, M. Minagawa, H. Yanagihara, M. Kishimoto, C. Mitsumata, S. Hashimoto, K. Yamada, and N. Ohkohchi, J. Phys. D: Appl. Phys. **43**, 474011 (2010).
[14] E. Myrovali, N. Maniotis, A. Makridis, A. Terzopoulou, V. Ntomprougkidis, K. Simeonidis, D. Sakellari, O. Kalogirou, T. Samaras, R. Salikhov, M. Spasova, M. Farle, U. Wiedwald, and M. Angelakeris, Sci. Rep. **6**, 37934 (2016).
[15] Z. Nemati, J. Alonso, L. M. Martinez, H. Khurshid, E. Garaio, J. A. Garcia, M. H. Phan, and H. Srikanth, J. Phys. Chem. C **120**, 8370 (2016).
[16] Z. Hedayatnasab, F. Abnisa, and W. M. A. Wan Daud, Mater. Sci. Eng. C **334**, 012042 (2018).
[17] D. D. Thongam, J. Gupta, N. K. Sahu, and D. Bahadur, J. Mater. Sci. **53**, 1110 (2018).
[18] T. Dayakar, K. Venkateswara Rao, K. Bikshalu, V. Rajendar, and S.-H. Park, Mater. Sci. Eng. C **75**, 1472 (2017).
[19] J. Gupta and, D. Bahadur, ACS Omega **3**, 2956 (2018).
[20] X. Yang, C. Zhang, A. Li, J. Wang, and X. Cai, Mater. Sci. Eng. C **95**, 104 (2019).
[21] J. E. Eixenberger, C. B. Anders, K. Wada, K. M. Reddy, R. J. Brown, J. Moreno-Ramirez, A. E. Weltner, C. Karthik, D. A. Tenne, D. Fologea, and D. G. Wingett, ACS Appl. Mater. Interfaces **11**, 24933 (2019).
[22] A. Woźniak, B. F. Grzeèkowiak, N. Babayevska, T. Zalewski, M. Drobna, M. W. Budych, M. Wiweger, R. Słomski, and S. Jurga, Mater. Sci. Eng. C **80**, 603 (2017).
[23] J. Gupta and D. Bahadur, ACS Sus. Chem. Eng. **5**, 8702 (2017).
[24] S. Seong, Y. C. Jung, T. Lee, I. -S. Park, and J. Ahn, Curr. Appl. Phys. **16**, 1564 (2016).
[25] X. Liu, C. Wang, X. Wang, C. Tian, Y. Shen, and M. Zhu, Mater. Sci. Eng. C **118**, 111455 (2021).
[26] H. Zhang, N. Patel, S. Ding, J. Xiong, and P. Wu, Biomater. Sci **4**, 288 (2016).
[27] S. B. Atla, W.-R. Lin, T.-C. Chien, M.-J. Tseng, J.-C. Shu, C.-C. Chen, and C.-Y. Chen, Chem. Phys. **216**, 380 (2018).
[28] S. H. Ammar, W. A. Abdulnabi, and H. D. A. Kader, Environ. Nanotechnol. Monit. Manage. **13**, 100289 (2020).
[29] S. Sun and H. Zeng, J. Am. Chem. Soc. **124**, 8204 (2002).
[30] L. Lu, W. Zhang, D. Wang, X. Xu, J. Miao, and Y. Jiang, Mater. Lett. **64**, 1732 (2010).
[31] K. C. Barick and D. Bahadur, J. Nanosci. Nanotechnol. **7**, 1945 (2007).
[32] C. T. Dung, L. M. Quynh, T. T. Hong, and N. H. Nam, VNU J. Sc.: Math. Phys. **33**, 14 (2017).
[33] S. B. Atla, W.-R. Lin, T.-C. Chien, M.-J. Tseng, J.-C. Shu, C.-C. Chen, C.-Y. Chen, Mater. Chem. Phys. **216**, 380 (2018).
[34] M. Kallumadil, M. Tada, T. Nakagawa, M. Abe, P. Southern, and Q. A. Pankhurst, J. Magn. Magn. Mater. **321**, 1509 (2009).
[35] S. Rana, K. C. Barick, and P. A. Hassan, J. Nanofluid **4**, 421 (2015).